Landscape modelling of the Yalong River catchment during the uplift of Southeast Tibet

Xiong Ou, Anne Replumaz

▶ **To cite this version:**

Xiong Ou, Anne Replumaz. Landscape modelling of the Yalong River catchment during the uplift of Southeast Tibet. Earth and Planetary Science Letters, 2024, 637, 10.1016/j.epsl.2024.118721 . insu-04604397

HAL Id: insu-04604397

https://insu.hal.science/insu-04604397v1

Submitted on 25 Nov 2024

HAL is a multi-disciplinary open access archive for the deposit and dissemination of scientific research documents, whether they are published or not. The documents may come from teaching and research institutions in France or abroad, or from public or private research centers.

L'archive ouverte pluridisciplinaire **HAL**, est destinée au dépôt et à la diffusion de documents scientifiques de niveau recherche, publiés ou non, émanant des établissements d'enseignement et de recherche français ou étrangers, des laboratoires publics ou privés.

Landscape modelling of the Yalong River catchment during the uplift of Southeast Tibet

Xiong Ou[1] and Anne Replumaz[1]

[1] Institut des Sciences de la Terre (ISTerre), Université Grenoble Alpes, CNRS, IRD, UGE, Grenoble, 38058, France

Correspondence to: Xiong Ou (xiong.ou@univ-grenoble-alpes.fr) and Anne Replumaz (anne.replumaz@univ-grenoble-alpes.fr)

Citation: Ou, X. and A. Replumaz, Landscape modelling of the Yalong River catchment during the uplift of Southeast Tibet, EPSL, doi:10.1016/j.epsl.2024.118721, 2024

Abstract.

Southeast Tibet is characterized by low–relief surfaces at high–elevation, showing very little exhumation during the India–Asia collision, as well as deeply incised rivers valleys. Understanding how these low–relief surfaces adjacent to the plateau's edge survived from regressive fluvial erosion is still an enigma, which is key to understanding the formation of the plateau. In the Three Rivers Region around the Eastern Himalayan Syntaxis, the squeezing of the Salween, Mekong and Yangtze rivers' drainage basins in their middlestream, where numerous thrusts parallel to the river channels are observed, has been invoked as the key factor driving the river evolution. More to the east, in the Great Bends Region, no such squeezing of the drainage basins has been observed; the Yalong and Yangtze rivers flow perpendicularly across northeast–trending thrust belts, generating huge (>100 km) river course bends with steep channel slopes. These faults have significantly contributed to construct the high plateau margin, including the Yalong Thrust Belt (YTB), active during the Eocene (~35–25 Ma) and reactivated in the Miocene (15–12 Ma). By applying state–of–the–art landscape modelling (FastScape) to the Yalong River catchment, with simplified rock uplift scenario deduced from fault activities, we show that strong monsoonal precipitation on the plateau (~1 m/yr), even during only a short period such as the Mid–Miocene Climatic Optimum (17–14 Ma), produces wide rivers and destroys the plateau edge. In contrast, modelling the orographic effect with weak net precipitation (~0.2 m/yr) above ~2700 or 4000 m, preserves the plateau edge and reproduces the slope of the Yalong River, but with a width larger than in nature. To reproduce both the slope and narrowness of the Yalong gorge just upstream of the YTB, a combination of a rapid Miocene rock uplift leading to a regional surface uplift, which creates a significant orographic effect and preserves interfluve low–relief surfaces close to the plateau edge, and a water inflow in upstream, which deeply incises downstream river valleys, is necessary. Such an amount of upstream water is collected from the flat and expansive headwater, inherited from the inland endorheic zone of the plateau interior, on which the hillslope processes dominate the landscape evolution.

Keywords: **Southeast Tibet, Yalong River catchment, Yalong River Gorges, Low–relief Surfaces, Landscape Evolution modelling, FastScape.**

1. Introduction

The western half of the immense and elevated (~5000 m on average) Tibetan Plateau is characterized by a vast low–relief endorheic zone (Fig. 1A). Numerous and extensive lacustrine sediments dated between ~23.5 Ma and ~13.5 Ma suggest that the endorheic zone of the plateau extended further to the east in the Miocene (Wu et al., 2008, Fig. 1B). In contrast, the eastern half at present–day is externally drained by large rivers, such as the Salween, Mekong, Yangtze and Yalong, with low–relief upstream areas on the plateau and low–relief interfluve surfaces perched at high elevation (~4500 m on average) along >2000 m deep gorges across the plateau edge. A strong interaction between tectonic and climatic forcing is expected to sculpt the characteristic relief and drainage network of the southeastern Tibetan Plateau. First, at the continental scale, it has been proposed that the Eastern Asian monsoon and the inner Asian desertification have been established in the Eocene since ~35 Ma following the growth of the Tibetan Plateau under the tectonic forcing of the Indian indentation into the Asia since ~50 Ma (e.g., Sorrel et al., 2017; Zheng et al., 2022), with a strengthening of the climatic contrast on the Eurasian continent in the Miocene since ~22 Ma (e.g., Clift, 2006; Clift and Giosan, 2014; Fang et al., 2021). At present–day, a strong orographic effect is observed, with more than 1.5 m/yr in the foreland below ~1000 m to less than 0.5 m/yr in the highland above ~2700 m (Fig. 1). Second, in Southeast Tibet, the intriguing low–relief surfaces close to the plateau edge, with little denudation during the plateau uplift, have been extensively studied to understand the plateau formation. They have been interpreted either as passive markers of the uplift of Southeast Tibet with contemporaneous river incision since ~13 Ma (e.g., Clark et al., 2005; Zhang et al., 2022), or as remnant abrasion surfaces incised by regressive fluvial erosion lagging behind the plateau uplift (Liu-Zeng et al., 2008).

Quantitative landscape evolution models have been proposed to study such tectonic/climatic forcing interaction in Southeast Tibet, testing different fluvial incision parameters and varying rock uplift in space and time (e.g., Yang et al., 2015; Fox et al., 2020; Yuan et al., 2021; Yuan et al., 2022; Yuan et al., 2023). Drainage area squeezing by lateral advection during the plateau uplift (Hallet and Molnar, 2001) and divide migration or river capture (Clark et al., 2004) have also been suggested to drive the river's evolution. In this paper, we propose landscape evolution models in which several parameters are constrained by morphotectonic and climatic observations in what we call the Great Bends Region. Indeed, in Southeast Tibet, two zones can be distinguished (Fig. 2). In the so–called Three Rivers Region, thrusts are trending north–south and parallel to the river channels, generating a strong lateral squeezing of the drainage basins of the Salween, Mekong and Yangtze rivers in their middlestream. But in the Great Bends Region, thrusts are trending north–east and perpendicular to the river channels of the Yangtze and Yalong rivers, generating huge river course bends of more than 100 km long, where spectacular gorges are observed (Fig. 2C). The Yangtze River flows through these two zones, with a complex catchment geometry showing both lateral squeezing in its middlestream and a huge bend across the Yulong thrust in its downstream. In contrast, the Yalong River catchment has a very simple rectangular shape, showing no squeezing and no river capture upstream of the bend across the Muli thrust (Fig. 2B). Here, we aim to model the landscape evolution of the Yalong River catchment in the Great Bends Region, by using FastScape (Braun and Willett, 2013). We study how the tectonic/climatic interaction leads to the deeply carved gorges and the preservation of low–relief surfaces in the headwaters and interfluves of the southeastern plateau edge upstream of the thrust faults, by testing both the influence of tectonic (rock uplift) and climatic forcing (i.e. precipitation, monsoon initiation, orographic effect).

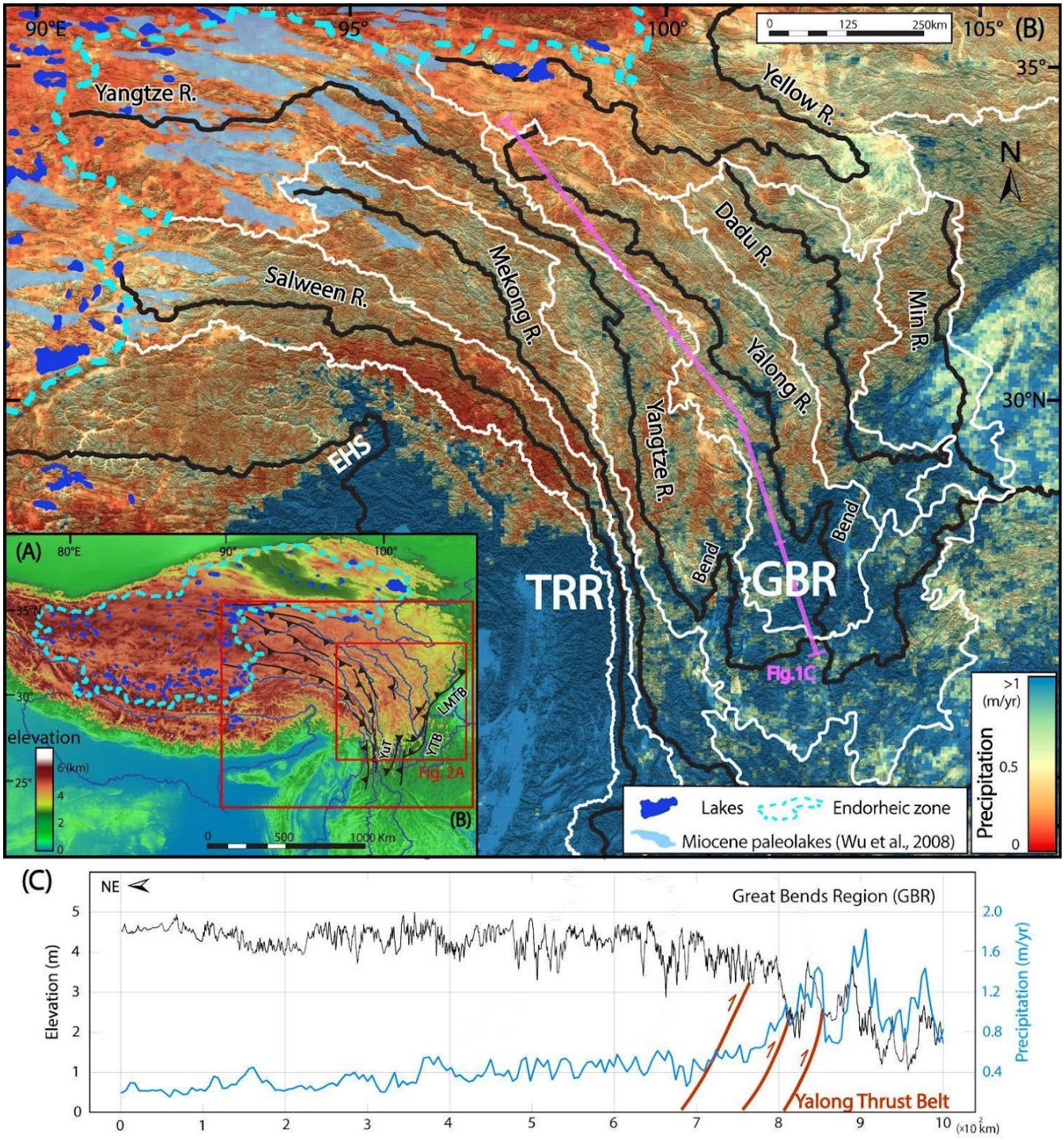

***Figure 1**: (A) Topography of the Tibetan Plateau with large externally drained rivers (blue lines) in the southeastern region and a vast endorheic zone in the northwestern region (cyan dashed line). LMTB: Longmenshan Thrust Belt, YTB: Yalong Thrust Belt, YuT: Yulong Thrust. (B) Precipitation map of Southeast Tibet based on TRMM 2B31 (1998–2009) dataset. Thick white lines delimit the different river catchments. TRR: Three Rivers Region. GBR: Great Bends Region. EHS: Eastern Himalayan Syntaxis. R.: river (C) Precipitation and topography profiles across the Yalong River catchment (pink line in B), showing a gradual increase of topography and a sharp decrease of precipitation toward northwest across the Yalong Thrust Belt.*

2. Regional Cenozoic geological setting

2.1 Externally drained Southeast Tibet: Great Bends Region versus Three Rivers Region

The externally drained Southeast Tibet can be divided in two zones, where tectonics differently influence river drainage networks. In the Great Bends Region, the Yangtze and Yalong rivers display spectacular bends (> 100 km) where they cross perpendicularly the north–east trending Yulong Thrust and Yalong Thrust Belt (YTB), respectively (Fig. 2). The Yulong thrust was only active between 28–20 Ma with exhumation rates of 0.57–0.8 km/Myr (Cao et al., 2019). Within the YTB, the Jiulong thrust was active during 35–30 Ma then re–activated during 9–6 Ma, with exhumation rates of 0.5 km/Myr and 0.6 km/Myr, respectively (Zhang et al., 2016). The Muli thrust was active since 50 Ma, with an exhumation rate of 0.2 ± 0.06 km/Myr, increasing to a maximum of 0.6 ± 0.08 km/Myr near the fault since 12.5 ± 1 Ma (Pitard et al., 2021). The Jinghe–Qinhe thrust is less well constrained, active either during 17–5 Ma (Wang et al., 2012b) or during 20–16 Ma with an exhumation rate of 0.4 km/Myr (Zhu et al., 2021). A large knickzone with steep slope (>200 km) is observed along the Yalong River bend upstream of the YTB (Fig. 2A), when crossing the topographic jump between the foreland and the plateau (Fig. 1C). More to the east, a smaller knickzone with less steep slope is observed along the Dadu River, along a smaller bend when crossing the Longmenshan Thrust Belt (LMTB). The activity of the LMTB was roughly synchronous to that of the YTB, with the first Oligocene phase (exhumation rate 0.8 km/Myr during 30–25 Ma) more intense than the second Miocene phase (exhumation rate 0.4 km/Myr during 10–0 Ma) (Godard et al., 2009; Wang et al., 2012a).

The Three Rivers Region corresponds to the arcuate drainages of the upstream Yangtze, Mekong and Salween rivers that flow around the Eastern Himalayan Syntaxis, parallel to each other with a spacing of only a few tens of kilometers (Fig. 1). Such a narrow spacing between large rivers has been interpreted as indicating strong regional northeastward shortening in response to the indentation of the Eastern Himalayan Syntaxis (Hallet and Molnar, 2001), accommodated by parallel north–west/north striking thrusts, which guide the rivers orientation (Replumaz et al., 2020). Modelling a dataset of multiple low–temperature thermochronometers indicated a decreasing erosion rate from west (Salween River) close to the Eastern Himalayan Syntaxis, to east (Yangtze River) away from it, since at least 10 Ma, suggesting a dominant tectonic forcing of compression perpendicular to the rivers (Yang et al., 2016). For the Kawagebo peak, the highest summit in the Three Rivers Region, the tectonic forcing is also dominant, uplifted since ~10 Ma in a restraining overstep between the Parlung and Zhongdian strike-slip faults (Ou et al., 2021, Fig. 2C). A very large knickzone (e.g., >300 km along the Mekong River), with less steep slope than measured for the Yalong River, is observed in the Three Rivers Region, upstream of the Kawagebo peak (Fig. 2A).

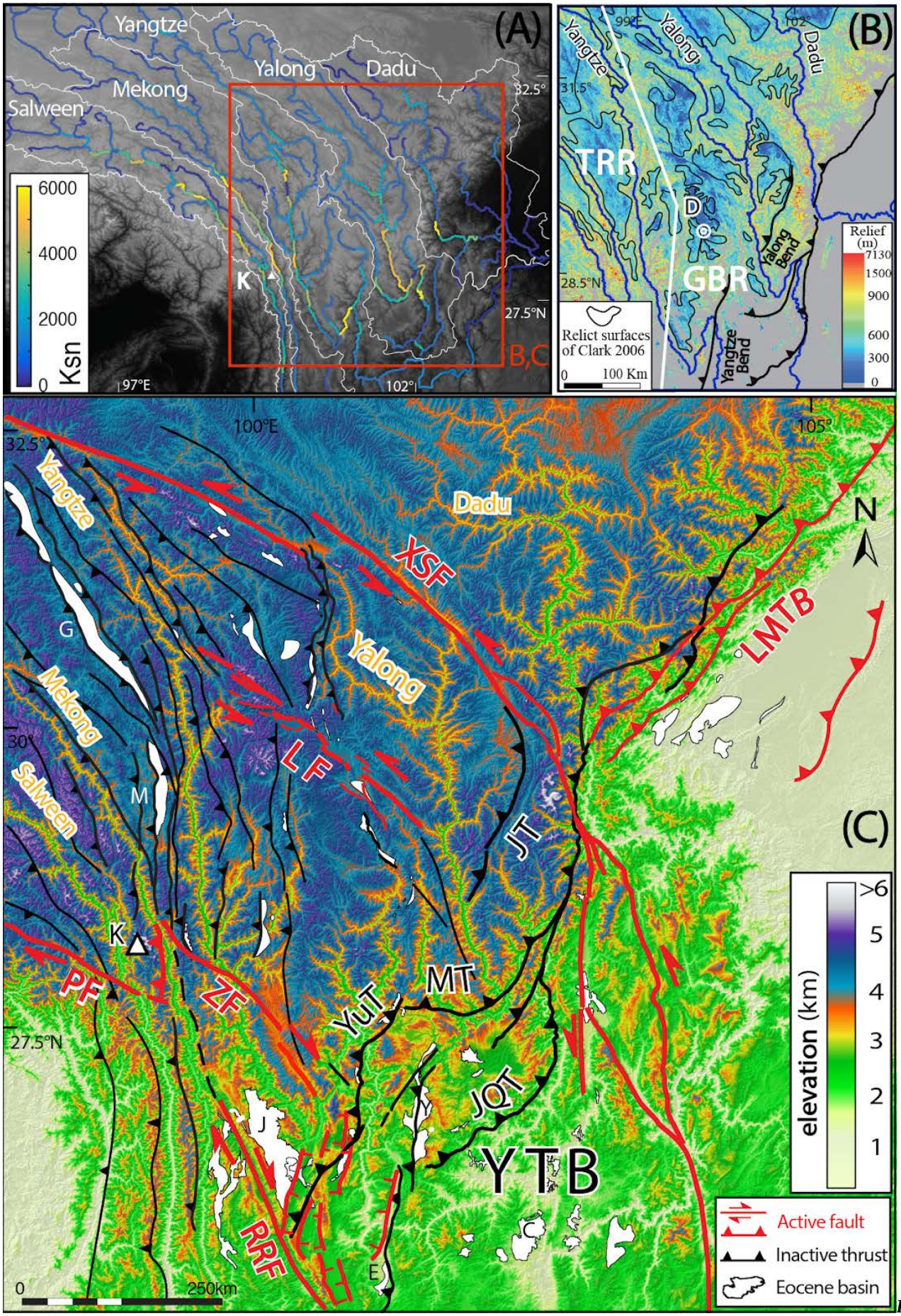

Figure 2*: (A) normalized steepness index (k_{sn})(Wobus et al., 2006; Kirby and Whipple, 2012) map of large rivers of Southeast Tibet. (B) Relief map of the eastern Tibetan Plateau (modified from Zhang et al., 2015). Rivers are marked in dark blue thick lines.*

The thick white line separates the Three Rivers Region (TRR) from the Great Bends Region (GBR). D: Daocheng city, on the most emblematic relict surface. (C) Topography of Southeast Tibet, showing the deeply entrenched rivers. Active faults: XianShuiHe (XSF), Litang (LF), Parlung (PF), Zhongdian (ZF), Red River (RRF), Longmenshan Thrust Belt (LMTB). Inactives thrusts: Muli (MT), Jiulong (JT), Jinhe–Qinghe (JQT) forming the Yalong Thrust Belt (YTB), Yulong (YuT). Basins: Chake (C), Eryuan (E), Gonjo (G), Jianchuan (J), Markam (M) and Yanyuan (Y).

2.2 Cenozoic climatic and tectonic evolution of Southeast Tibet: sedimentary and paleo–elevations data

In the epicontinental seas of East and Southeast Asia, a strong increase of sedimentation rates has been observed at ~40 Ma, interpreted as the start of the Southeast Tibet uplift (Clift, 2006). Inland, in the Three Rivers Region, infilling of several sedimentary basins during Eocene–Oligocene, including the Gonjo, Markam and Jianchuan basins (e.g., Cao et al., 2020; Gourbet et al., 2017; Li et al., 2015a; Su et al., 2019; Tang et al., 2017; Xiong et al., 2020), was also interpreted as marking the onset of the Southeast Tibet uplift near the Eastern Himalayan Syntaxis (Fig. 2C). In this region, paleoaltimetry studies from the Gonjo and Markam basins near the plateau edge showed that they have been at present day's elevation since ~40 Ma or ~30 Ma, respectively (Li et al., 2015a; Su et al., 2019; Tang et al., 2017; Xiong et al., 2020), while the foreland Jianchuan basin was uplifted since ~28 Ma to reach the modern height at ~20 Ma (Cao et al., 2020; Gourbet et al., 2017). In the Great Bends Region, paleo–elevation data is available only in the piedmont, with the Eryuan and Yanyuan basins reaching their present elevation of ~2300 m around 5 Ma, and the Chake Basin reaching ~2000 m at ~11 Ma (Hoke et al., 2014; Li et al., 2015b, Fig. 2C), suggesting that the main uplift phase started later than in the Three Rivers Region.

Another increase of sedimentation rates has been observed in epicontinental seas of East and Southeast Asia during the Miocene (~17–14 Ma), showing a strengthening of the summer monsoon since the Mid–Miocene Climate Optimum) (Guo et al., 2002, Guo et al., 2008; Clift, 2006). This climatic forcing has been interpreted as the main factor controlling the erosion history along the Mekong River (Nie et al., 2018). A drainage–area expansion of the large external rivers into the endorheic zone since 15–10 Ma, probably driven by the strengthening summer monsoon, has also been proposed to lead to increasing runoff, stream power and therefore enhanced erosion (Rohrmann et al., 2018, 2023). Erosion rates deduced from detrital thermochronometry averaged over the upstream catchments of major rivers, show rapid erosion between 11 and 4 Ma (Duvall et al., 2012), which has also been interpreted as capturing the upstream endoreic zone.

3. Method: Landscape evolution model (FastScape)

3.1 Landscape evolution modelling

In tectonically active regions, landscape evolution rate is principally set by the efficiency of bedrock river incision, with the steep slopes of such regions responding rapidly to river incision (Clark et al., 2004). We use FastScape (Braun and Willett, 2013), to solve the stream power law for bedrock river incision (Whipple and Tucker, 1999) and predict landscape evolution by testing tectonic (rock uplift) and climatic (precipitation) forcing. According to the stream power law, the height evolution of fluvial channels (dh/dt) depends on the difference between the rock

uplift rate (U) and the surface erosion rate (E), which is proportional to the local slope (S) and the drainage area (A), a proxy for river discharge (Howard and Kerby, 1983). Fluvial erosion is also interdependent with hillslope processes, which are subject to mass transport at a rate, commonly represented by linear diffusion proportional to the curvature of topography, by assuming mass conservation (Ahnert, 1967). The basic equation solved by FastScape is:

$$\frac{dh}{dt} = U - K_f p^m A^m S^n + K_d \left(\frac{d^2h}{dx^2} + \frac{d^2h}{dy^2} \right) \quad (1)$$

Where h is the elevation (m), t is the time (yr), U is the rock uplift rate (m/yr), K_f is the erodibility coefficient (m^{1-2m}/yr), p is the net precipitation rate (m/yr), A is the drainage area (m^2), S is the local channel slope, and m, n are the stream power model exponents. K_f, m and n depend on lithology, precipitation, channel width, flood frequency and channel hydraulics (Whipple and Tucker, 1999; Lague et al., 2005). The stream channel metric χ, calculated from the path integral of the inverse of the upstream drainage area raised to an exponent equal to the ratio of m/n, is used to normalize and to quantitatively compare river profiles independently from the variation of drainage area (Perron and Royden, 2013). The concavity ratio m/n have been constrained to 0.4 for the Salween, Mekong and Yangtze rivers by minimizing scatters between the χ–elevation plot of all tributaries (Yuan et al., 2021; Yuan et al., 2022; Yuan et al., 2023). Using this method, we obtain the same concavity ratio value for the Yalong River (Fig. S1 & S2). Tests with different n and m do not improve the results (Fig. S9). Empirical values for K_f range from 10^{-6} to 10^{-2} $m^{0.2}$/yr (e.g., Stock and Montgomery, 1999; Armitage et al., 2018), and have been tested in our models. K_d is the hillslope sediment transport coefficient or diffusivity (m^2/yr), ranging from 10^{-4} to 10^{-1} m^2/yr (Martin, 2000). A K_d equal to 10^{-2} m^2/yr is adopted in our models, as proposed in Densmore et al. (2007), after exploring various values of it (Fig. S11). In this paper, we use forward landscape evolution modelling, testing erodibility coefficient (K_f), with varying rock uplift and precipitation rates in space and time (U and p) to model the topographic evolution of the Yalong River catchment.

3.2 Model setup

The model setup is based on a rectangle of 1250 km in length and 200 km in width, similar to the Yalong River catchment, discretized by 1250 × 200 regularly spaced nodes (Fig. 3B). All models in our study were run for a period of 50 Ma, the approximative onset timing of Asian–Indian collision. The time step is set to be 200 ka, so that models run for 250 time steps. The initial elevation is constant and set to 1000 m, corresponding to the altitude of the outlet of the Yalong River catchment. The downstream boundary is the only outlet of the model domain, with a constant base–level elevation at 900 m. A small initial channel is emplaced in the middle of the foreland perpendicular to this downstream boundary, mimicking Yalong River's outlet (Fig. 3A). The upstream boundary is reflecting, meaning that water is reflected in the opposite direction, with no water flowing out through this limit. The lateral boundaries are periodic, meaning that nodes on one boundary have nodes on the other boundary as neighbors (Braun and Willett, 2013). Rock uplift rate and precipitation, the two principal parameters in our models, can vary in time and in space. For the rock uplift rate, the model is separated in 2 zones, upstream and downstream of the Muli Thrust, located at 150 km from the downstream boundary. Only variations of the rock uplift rate upstream of the fault are tested. For the precipitation, several zones and rates are tested.

We analyze the model outputs of FastScape with the topographic analysis tool Topotoolbox2 (Schwanghart and Scherler, 2014). For the chosen time–steps in outputs, we plot channel elevation versus χ for a comparison between modelled and observed river profiles. Cross–sections of the river valleys and 20–km wide swath profiles along the river channel are extracted to compare the geometry of modelled river valleys to the deeply incised Yalong River gorge. The normalized channel steepness index (k_{sn}), representing the gradient of channel elevation with respect to χ, is also calculated for the river profiles (Kirby and Whipple, 2012; Wobus et al., 2006).

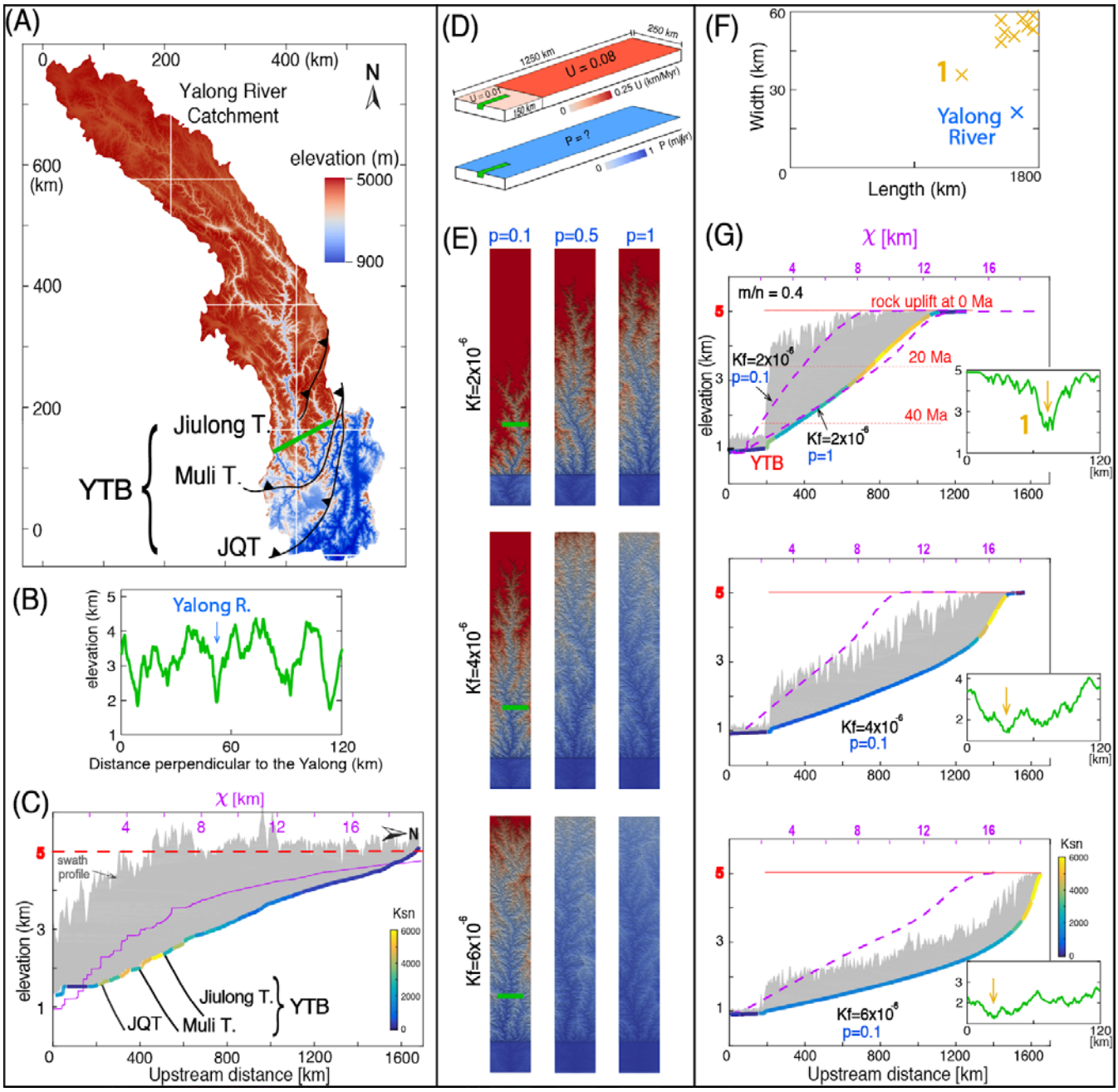

***Figure 3**: (A) Topography of the Yalong River catchment. (B) Cross–section topography perpendicular to the channel along the green line in A. (C) 20–km wide swath topographic profile (grey patch), k_{sn} values and χ-elevation profile (purple line) along the Yalong River. YTB: Yalong Thrust Belt, including Jiulong, Muli and Jinghe–Qinhe (JQT) thrusts (T.). (D) Model setup: a 1250 × 200 km box with spatially variable rock uplift rate (U) in red and constant precipitation (p) in blue. (E) Final state topography of models with different K_f ($m^{0.2}$/yr) and p (m/yr). (F) Plot of valley width versus length of the Yalong (in blue) and modelled rivers (in orange), with valley width measured along the green lines on the topographic maps in A and E.*

(G) 20–km wide swath profiles (grey patches), k_{sn} values and χ profile (dashed purple lines) of the modelled rivers in E with p=0.1 m/yr. Rock uplift with time (red line). Inset boxes show topographic cross–sections along green lines in E.

4. Landscape evolution results testing erodibility, rock uplift and precipitation rates

The upstream low–relief area of the Yalong River catchment lies at an average elevation of ~5000 m, gradually decreasing southeastward to ~2000 m (Fig. 3A). The YTB delimits a knickzone with a high value of k_{sn}, where the river has downcut narrow and deep valley, with a local relief >2500 m (Fig. 3B, C). By using forward landscape evolution modelling, we test erodibility (K_f), with varying rock uplift and precipitation rates in space and time (U and p), based on scenarios proposed for Southeast Tibet and on our own geomorpho-tectonic analysis of the Yalong River catchment. We aim to obtain the best agreement with observed topography of the Yalong River catchment, and conclude on the tectonic/climatic forcing interaction in the region.

4.1 Basic parametric study: testing erodibility and precipitation rate

A constant rock uplift rate of 0.08 km/Myr is imposed upstream of the thrust to reach a maximum total rock uplift of 5000 m during 50 Ma, while a slow rock uplift rate of 0.01 km/Myr is imposed downstream (Fig. 3D). We test different values of K_f and p. Results show that increasing K_f and/or p strengthens regressive erosion, with the slope of the mainstem river channel varying from nearly linear to convex–up (Fig. 3G). Precipitation of 0.1 m/yr and a small K_f of 2×10^{-6} $m^{0.2}$/yr are insufficient to propagate river erosion to the plateau interior, producing a short linear river and χ profiles, with low–relief interfluve surfaces at high elevations and intact flat surfaces in high headwaters (Fig. 3E). In contrast, a K_f value of 6×10^{-6} $m^{0.2}$/yr erodes the whole region even with low precipitation (0.1 m/yr), creating a strongly convex–up river and χ profiles and leaving almost no high channels or surfaces preserved along the river. With a medium value of K_f of 4×10^{-6} $m^{0.2}$/yr, the model reproduces relatively well the river channel convexity and some well–preserved high topography. When increasing the K_f value, the width of the modelled river valleys also increases, shifting from a narrow and deep valley to a broad one (insets in Fig. 3G). Nevertheless, none of these modelled rivers reproduce the narrowness of the downstream Yalong River, and the modelled narrowest one is not as long as the natural case (Fig. 3F, G). Furthermore, the high k_{sn} values are located upstream on the modelled river profiles, showing localized intense erosion in the upstream–most part, contrasting with the knickzone located at the edge of the plateau when crossing the YTB in the natural case (Fig. 3G).

4.2 Tectonic forcing: Jiulong and Muli uplift scenarios

We test a scenario with a rock uplift phase during 30–0 Ma with a rate of 0.13 km/Myr, representing exhumation rate since the Late Eocene–Oligocene observed on the Jiulong thrust (Zhang et al., 2016), named “Jiulong uplift scenario” (Fig. 4A). We also test a strong rock uplift rate of 0.24 km/Myr since 15 Ma, representing the middle Miocene exhumation phase revealed for the Muli thrust (Pitard et al., 2021), named “Muli uplift scenario” (Fig. 4B). Prior to the onset of thrust activity, a protracted phase with low rock uplift rate of 0.01 km/Myr is applied everywhere in the models. A constant strong precipitation of 1 m/yr since 50 Ma is employed in both scenarios

considering a middle Eocene onset of the Inter–Tropical Convergence Zone (ITCZ)–induced monsoon (e.g., Sorrel et al., 2017; Zheng et al., 2022).

Results show that a long rock uplift phase since 30 Ma with a relatively small rate favors strong regressive erosion in channels, creating strongly concave–up rivers, no matter which K_f value is applied (Fig. 4E, see also systematic tests in supplementary materials, Fig. S3). However, a higher rock uplift rate during a shorter period of 15 Ma roughly reproduces river and χ–elevation profiles similar to the Yalong River, when applying a K_f of 4×10^{-6} $m^{0.2}$/yr (Fig. 4F, S3). Nevertheless, the k_{sn} values are higher along the entire modelled profile than in nature, the width of the modelled river valley is much larger than the narrow and steep one of the Yalong River, and few high topography is preserved at the edge of the plateau. When using a lower K_f of 3×10^{-6} $m^{0.2}$/yr, high values of k_{sn} are observed close to the plateau edge, but the propagation of rivers into hinterland is limited and the river and χ–elevation profiles are placed much higher than the Yalong River. When using a higher K_f of 5×10^{-6} $m^{0.2}$/yr the modelled river incises more deeply than the Yalong River, with generally lower k_{sn} values and lower χ–elevation profile.

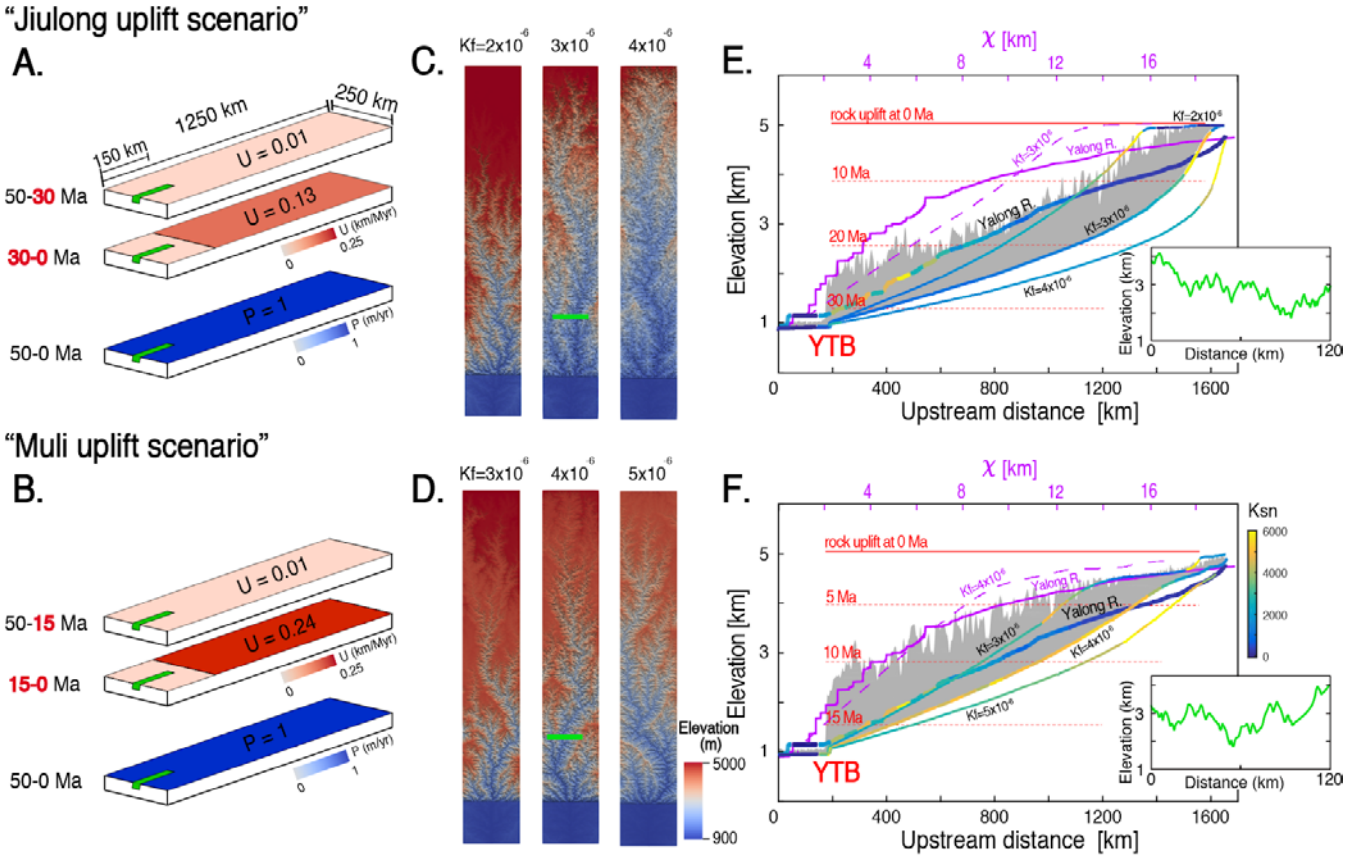

***Figure 4**: Testing tectonic forcing based on exhumation rate of Jiulong or Muli thrusts since the Late Eocene–Oligocene. Same legend as Figure 3. (A) "Jiulong uplift scenario" with U=0.13 km/Myr since 30 Ma, p=1 m/yr. (B) "Muli uplift scenario" with U=0.24 km/Myr since 15 Ma, p=1 m/yr. (C), (D) final topographic map of models with different K_f. (E) k_{sn} values for different K_f. χ profiles for $K_f=3\times10^{-6}$ $m^{0.2}$/yr. (F) k_{sn} values for different K_f. χ profiles for $K_f=4\times10^{-6}$ $m^{0.2}$/yr. See Fig. S3 for more models with different precipitation rates and K_f values.*

4.3 Climatic forcing: Mid-Miocene Climate Optimum and Top-down incision scenarios

We test a scenario that includes monsoonal strengthening during the Mid–Miocene Climate Optimum (~17–14 Ma) on a high plateau (~5000 m), which has been suggested to explain enhanced exhumation in the Mekong River valley during that period, solely due to climatic forcing (Nie et al., 2018). We denote this scenario as the "Mid–Miocene Monsoon scenario". Rock uplift at a rate of 0.13 km/Myr from 50–20 Ma creates a high plateau at ~5000 m under arid conditions (p=0.2 m/yr), before shifting to a wet monsoonal condition, with a strengthened precipitation (p=1 m/yr) (Fig. 5A). Precipitation rates between 0.4 and 1 m/yr have been tested (Fig. S4). All these models show that the plateau is strongly eroded by efficient regressive erosion due to enhanced monsoonal precipitation (Fig. 5C), with a drastic decrease of the maximum topography between 17 and 0 Ma (Fig. 5E). Only a few high surfaces at ~5000 m are preserved upstream, with a ubiquitously flat foreland. The river and χ profiles are strongly concave–up with a significant knickzone and highest k_{sn} values on the edge of the residual plateau (Fig. 5E), no matter which K_f value is applied (Fig. S4).

We also test a scenario with enhanced runoff and stream power in channels through an upstream drainage capture from the endorheic zone on the high plateau near ~15 Ma (Rohrmann et al., 2018, 2023), denoted as the "Top–down incision scenario". Rock uplift at a rate of 0.13 km/Myr from 50–20 Ma produces a high endorheic plateau at ~5000 m, considering no precipitation for the upstream half of the model (Fig. 5B). Capture of the endorheic zone takes place at 15 Ma, reproduced as an upstream expansion of strong rainfall area, leading to increasing runoff in the channel. Precipitation rates between 0.4 and 1 m/yr have been tested (Fig. S4). All these models show that the plateau is strongly eroded by "escarpment–retreat"–like (Braun, 2018) regression of the maximum topography since 15 Ma (Fig. 5D), no matter which K_f value is applied (Fig. S4). For lower precipitation rates or smaller K_f values, such escarpment–retreat propagates less far upstream (Fig. S4). The final concave–up river and χ profiles and k_{sn} distribution is similar to the "Mid–Miocene Monsoon scenario", both not reproducing the natural case (Fig. 5).

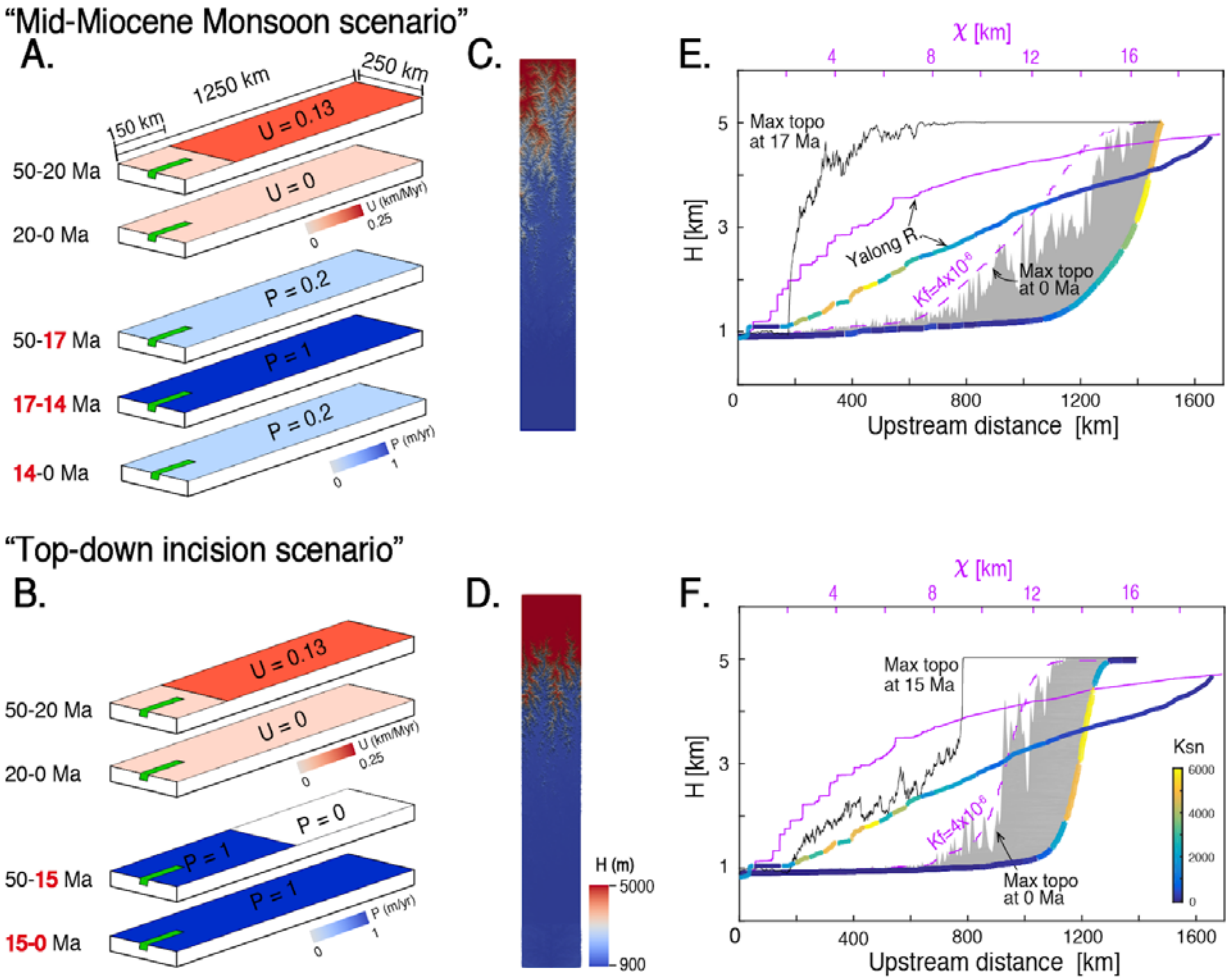

***Figure 5**: Testing climatic forcing. $K_f = 4\times10^{-6}$ $m^{0.2}$/yr. Same legend as Figure 3. (A) "Mid–Miocene Monsoon scenario" with monsoonal strengthening during the Mid–Miocene Climate Optimum (~17–14 Ma) on a high plateau (~5000 m) uplifted under arid conditions. (B) "Top–down incision scenario" with upstream drainage capture from the endorheic zone on the high plateau near ~15 Ma. (C), (D) final topographic state of the models. (E), (F) topography, k_{sn} and χ profiles of the modelled and Yalong rivers. The thin black lines represent the maximum topography in the y direction at 17 or 15 Ma before a climatic transition. See Fig. S4 for more models with different precipitation rates and K_f values.*

4.4 Climatic forcing: orographic effect scenarios

We test a dramatic drawdown of rainfall from 1 m/yr in the foreland to below 0.5 m/yr on the plateau as observed at present–day (Fig. 1), once the elevation of the plateau hinterland is above 2700 m, denoted as the "Orographic effect scenario". We choose to fit the present–day precipitation profile to the first order as a step, in agreement with a simplified step in our rock uplift regime (Fig. 6A). Considering that since when this orographic effect is observed and how the precipitation profile has evolved since 50 Ma are two major unknowns, we test an onset timing at 10 Ma when the plateau reaches ~2700 m high or at 5 Ma when the plateau reaches ~4000 m high (Fig. 6), considering a rock uplift of 0.24 km/Myr since 15 Ma, as in the "Muli uplift scenario". Various precipitation rates (0.1–0.5 m/yr) and K_f (4×10^{-6}–6×10^{-6} $m^{0.2}$/yr) have been tested (Fig. S5). When applying a K_f of 5 or 6×10^{-6} $m^{0.2}$/yr, most of these models, even with such a crude orographic effect, reproduce a river profile similar to the Yalong River one (Fig. 6). When $K_f = 4\times10^{-6}$ $m^{0.2}$/yr, wider low–relief and low–erosion surfaces at high elevation are preserved near

the plateau edge (Fig. S7). But none of these models reproduce the narrowness of the downstream Yalong gorge (Fig. 6 & S6). We also test some more complex precipitation scenarios, with the precipitation decreasing linearly with elevation or with precipitation stepping down away from the YTB, which doesn't better reproduce the Yalong River profile (Fig. S8).

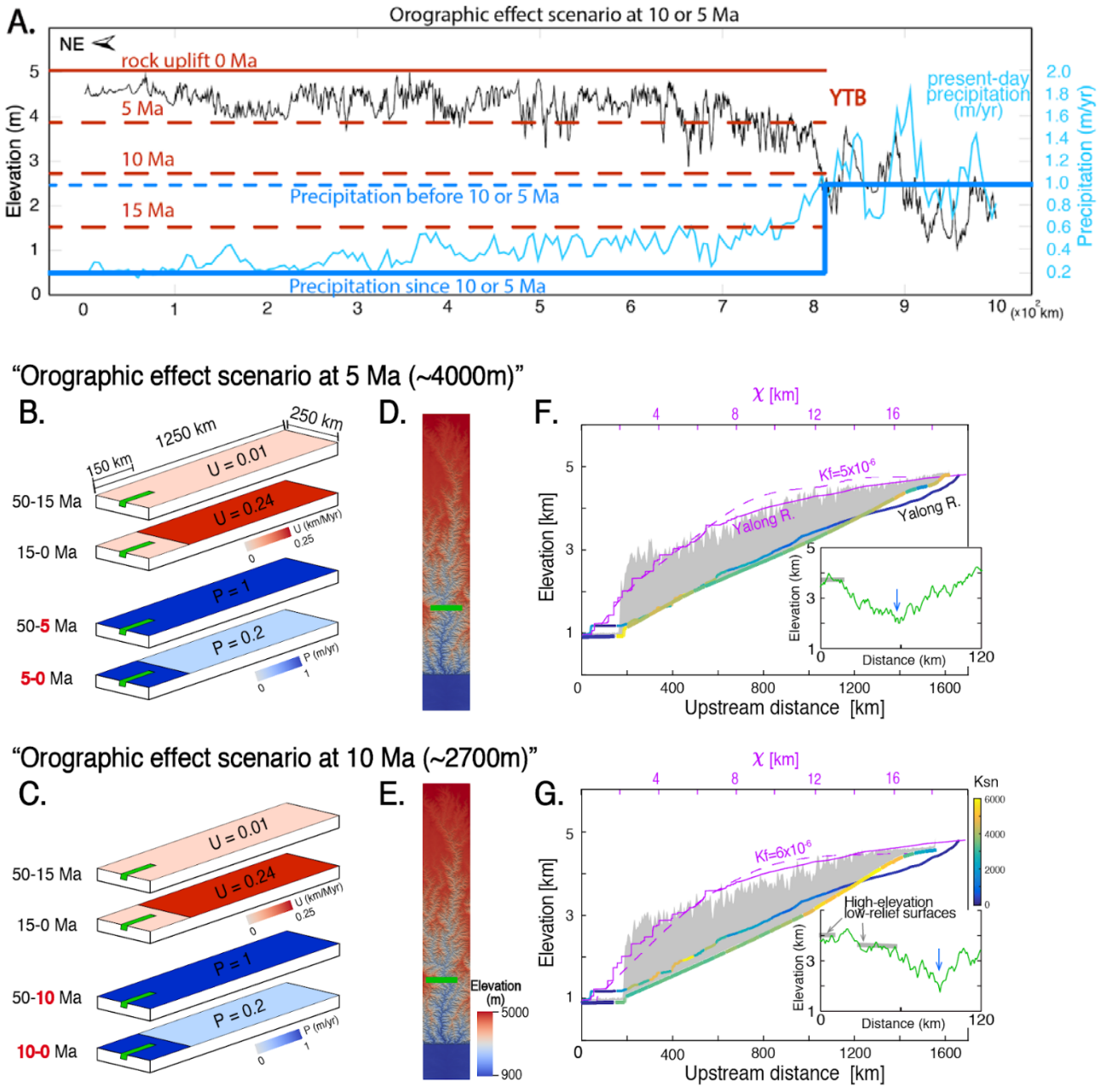

***Figure 6**: Testing the climatic forcing of the orographic effect, reproduced as a dramatic drawdown of rainfall once the elevation of the plateau hinterland is above 2700 or 4000 m, using an U as in the "Muli uplift scenario". Same legend as Figure 3. (A) Temporal variation of rock uplift and precipitation used, fitting to the first order the present–day precipitation profile. (B), (C) Model setting, precipitation drops to 0.2 m/yr when the plateau maximum elevation reaches 4000 m at 5 Ma (B) or 2700 m at 10 Ma (C). (D), (E) Final modelled topography; k_{sn} and χ profiles of the modelled and Yalong rivers with K_f of 5×10^{-6} $m^{0.2}$/yr (F) and 6×10^{-6} $m^{0.2}$/yr (G). Inset: topographic cross–section of river valley along green lines. See Fig. S5 & S7 for more models with different precipitation rates and K_f values.*

4.5 Combination of tectonic and climatic forcing: increasing upstream inflow scenario

Our former models reveal a contradiction between deep incision of river channels due to abundant runoff collected in the river network (Fig. 4) and preservation of flat high topography, for which weak upstream precipitation is mandatory (Fig. 6). We test a combination of a weak net precipitation (p=0.1 to 0.5 m/yr) on the most part of plateau since 10 Ma due to orographic effect on precipitation, and plentiful runoff in the channels, by incorporating a strong water inflow in the river network with an enhanced precipitation (W=0.4 to 1 m/yr) in the uppermost 450 km of the model (Fig. 7A). A combination of p=0.2 m/yr, K_f=4×10^{-6} m$^{0.2}$/yr and W=1 m/yr well reproduces a river channel similar to the Yalong River, with high–elevation and low–relief surfaces in the interfluves and headwaters, and a deep and narrow incised valley down to a depth of ~2500 m (Fig. 7). A comparison of valley width–river length plot of our models reveals that such an "increasing upstream inflow" scenario is the only one to reproduce the narrowness of the Yalong River (Fig. 7D). The highest k_{sn} values in this scenario occur near the thrust belt, similar to the knickzone upstream of the YTB in the Yalong River catchment (Fig. 7C). One thing to note is that the upstream–most section of the Yalong River profile (1/3 of all) shows a headward flattening of channel slope, marked by a small slope rupture, but this is not reproduced in our model. Models with K_f higher than 4×10^{-6} m$^{0.2}$/yr, show χ profiles slightly below the natural profile, over for lower K_f (Fig. S10C). For a K_f=4×10^{-6} m$^{0.2}$/yr, any precipitation value (p) reproduces more or less the natural river profile (Fig. S10A), but the precipitation of 0.2 m/yr models best the downstream river entrenchment (Fig. S10B). Varying the amount of upstream inflow (W) between 0.4 and 1 m/yr shows that larger values reproduce better the natural profile (Fig. S10E). Different durations of such a strong upstream inflow (W=1 m/yr) reveal that only a relatively long period (10–0 Ma) stimulates a comparable river profile and narrow downstream valley to the Yalong River (Fig. S10D). We also test various values of K_d=0.0001, 0.001, 0.01 and 0.1 m^2/yr, showing that K_d=0.01 m^2/yr, as recommended in Densmore et al. (2007), reproduces best the morphology of the Yalong River profile (Fig. S11).

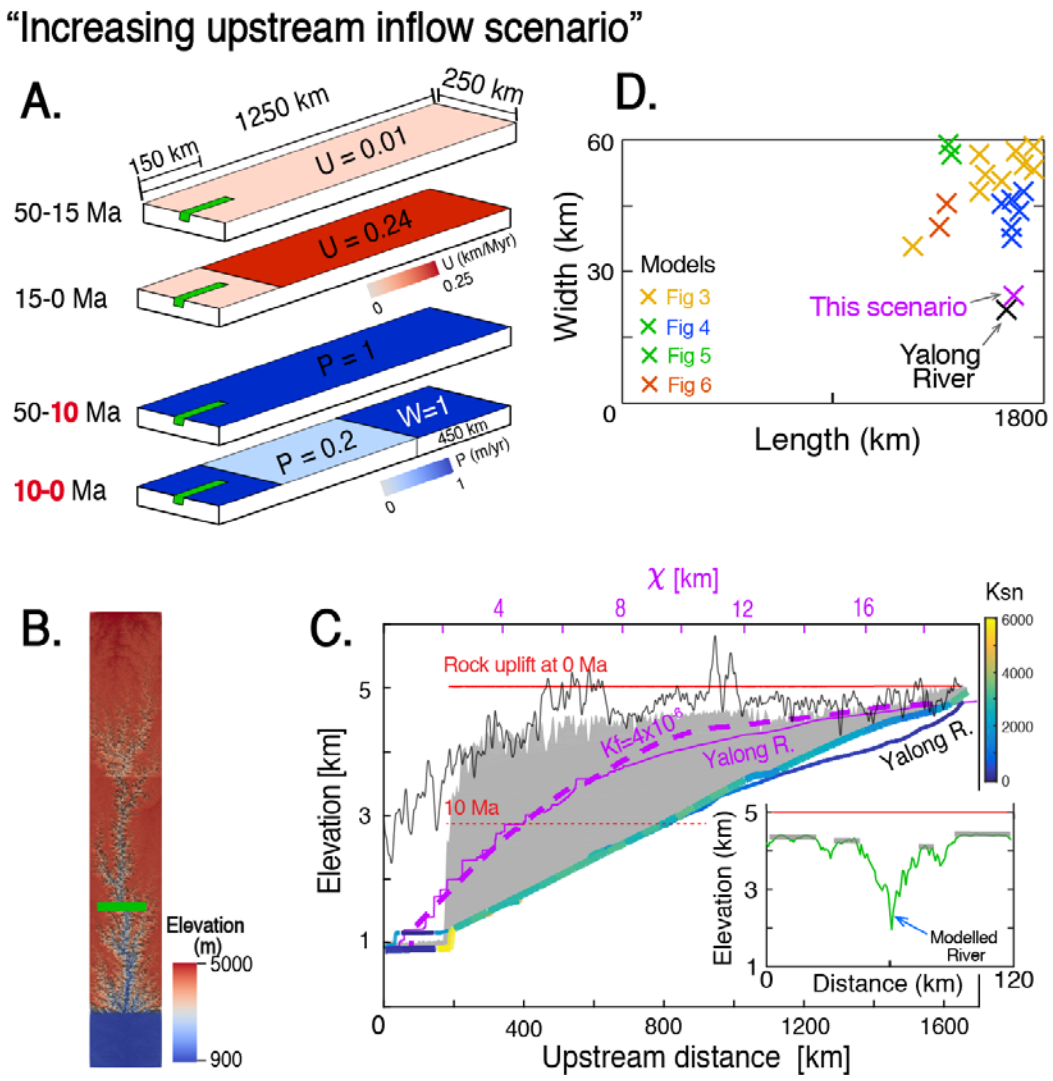

***Figure 7**: Testing a combination of tectonic and climatic forcing, with U as in the "Muli uplift scenario" and p as in the "orographic effect scenario" since 10 Ma. Same legend as Figure 3. (A) Model setting, W of 1 m/yr in the uppermost 450 km part, reproduces strong water inflow in the river network. K_f=4×10^{-6} m$^{0.2}$/yr. (B) Final topography. (C) topographic (black line), k_{sn} and χ profiles of the modelled and Yalong rivers. Inset: topographic cross–section of modelled river valley (green line in B), showing a deeply incised valley and preservation of a high plateau with thick grey lines showing the low–relief and high–elevation surfaces. (D) Plot of valley width, measured 200 km upstream of the YTB as in C, versus length of the Yalong River and all modelled rivers. See Fig. S10 for more models with different p, W and K_f, K_d values.*

5. Discussion: modelling long, deep and narrow river valleys with high and flat interfluves, as observed in Southeast Tibet

5.1 Comparing landscape evolution models of Southeast Tibet

In Southeast Tibet, the juxtaposition of high–elevation, low–relief interfluve surfaces (~4500 m high) close to the plateau edge and deeply–incised river valleys (~ 2500 m deep) in the middle reaches of large rivers (Fig. 8) has drawn attentions to how the interaction between climate and tectonics generates this peculiar landscape (e.g., Clark et al., 2005; Liu-Zeng et al., 2008). Several hypotheses have been proposed but they have been rarely modelled.

Using FastScape allows us to predict landscape evolution, where surface erosion rate depends mainly on river discharge and hillslope processes (Braun and Willett, 2013), and test simplified scenarios of rock uplift (tectonic forcing) and precipitation (climatic forcing). Our results show that with a constant rock uplift rate of 0.1 km/Myr during the collision (~50 Ma), high erodibility coefficient K_f and/or precipitation p favors regressive erosion throughout the river network, destroying the topography created and enlarging the valley width (Fig. 3). Even a short period of strong precipitation on an existing high plateau leads to a spectacular topographic decay by "escarpment–retreat" (Braun, 2018), leading to concave–up river profiles, different from the natural case (Fig. 5). We conclude that a scenario of monsoonal strengthening during the Mid–Miocene Climate Optimum (~17–14 Ma), with strong precipitation on a pre–existing high plateau, causing fast Miocene rock exhumation as previously proposed (Nie et al., 2018), would also cause such a topography decay. On the contrary, imposing both a fast rock uplift rate (0.24 km/Myr) since 15 Ma (e.g., Pitard et al., 2021) and drier condition at high altitude during the uplift of the plateau, reproducing to the first order the strong orographic effect observed at present–day (Fig. 1), is mandatory to obtain a comparable river profile to the Yalong's one and preserve the high and flat topography on the plateau edge (Fig. 8).

Another model of topographic evolution in the Three Rivers Region employed a wave of maximum rock uplift of 0.24 km/Myr propagating southeastward (Yuan et al., 2021), which is similar to the hypothesis of a lower crustal channel flow propagating from Central Tibet (Clark and Royden, 2000; Royden et al., 1997). It agrees to the first order with thermochronologic data showing earlier rock uplift to the north of the Three Rivers Region than in the south (~30 Ma for the Markam basin, Cao et al., 2020; ~20 Ma for the Jianchuan basin, Gourbet et al., 2017), and with paleoelevation of ~3800 +/- ~1000 m for the Markam basin since early Miocene (~23 Ma) while the Jianchuan basin elevation was only ~2600 +/1000 m at that time (Li et al., 2015a) . A strong p (1 m/yr) and a small K_f (1.2×10^{-6} $m^{0.2}$/yr) has been used in such "uplift wave model" to well reproduce the deeply incised river valleys and high flat surfaces in the headwaters and interfluves. Indeed, the strong precipitation on the plateau leads to enhanced runoff in the river network to carve deep valleys, while the downstreamward propagating uplift leads to a localized incision on the plateau edge, which avoids extensive erosion of uplifted high topography in hinterland. This scenario has been related to the lateral advection in the Three River Region, revealed by the narrow spacing between major rivers (e.g., Hallet and Molnar, 2001; Yang et al., 2015), which significantly affects the shape of rivers' catchment (Fig. 1B). Nevertheless, both the lateral advection and the southeastward propagation of uplift wave are not evidenced in the Great Bends Region by either paleoaltimetric or thermochronological data, while similar river profiles among the Yalong, Yangtze, Mekong and Salween rivers (Yang et al., 2016) suggest that a common process is needed. Furthermore, this model is not considering the observed strong orographic effect (Fig. 1).

Another approach, using inversion of normalized channel steepness and landscape response time to test the continuity of low–relief surfaces across Southeast Tibet, reveals discontinuity in channel steepness at the prominent bends of the Dadu and Yalong rivers, which have been interpreted as resulting from capture events (Fox et al., 2020). Indeed, numerous captures have shaped the present–day regional drainage pattern, but major captures occurred downstream of the river bends (e.g., Clark et al., 2004), while upstream drainage areas of the Yalong river show a very regular shape, suggesting minor influence of capture (Fig. 1). In the Great Bends Region, such downstream captures could influence the k_{sn} value at the river bend, and also the slope of river channel, but they

should not be the dominant process for preserving the low–relief surfaces above the YTB and generating the narrowness of gorges at the plateau edge.

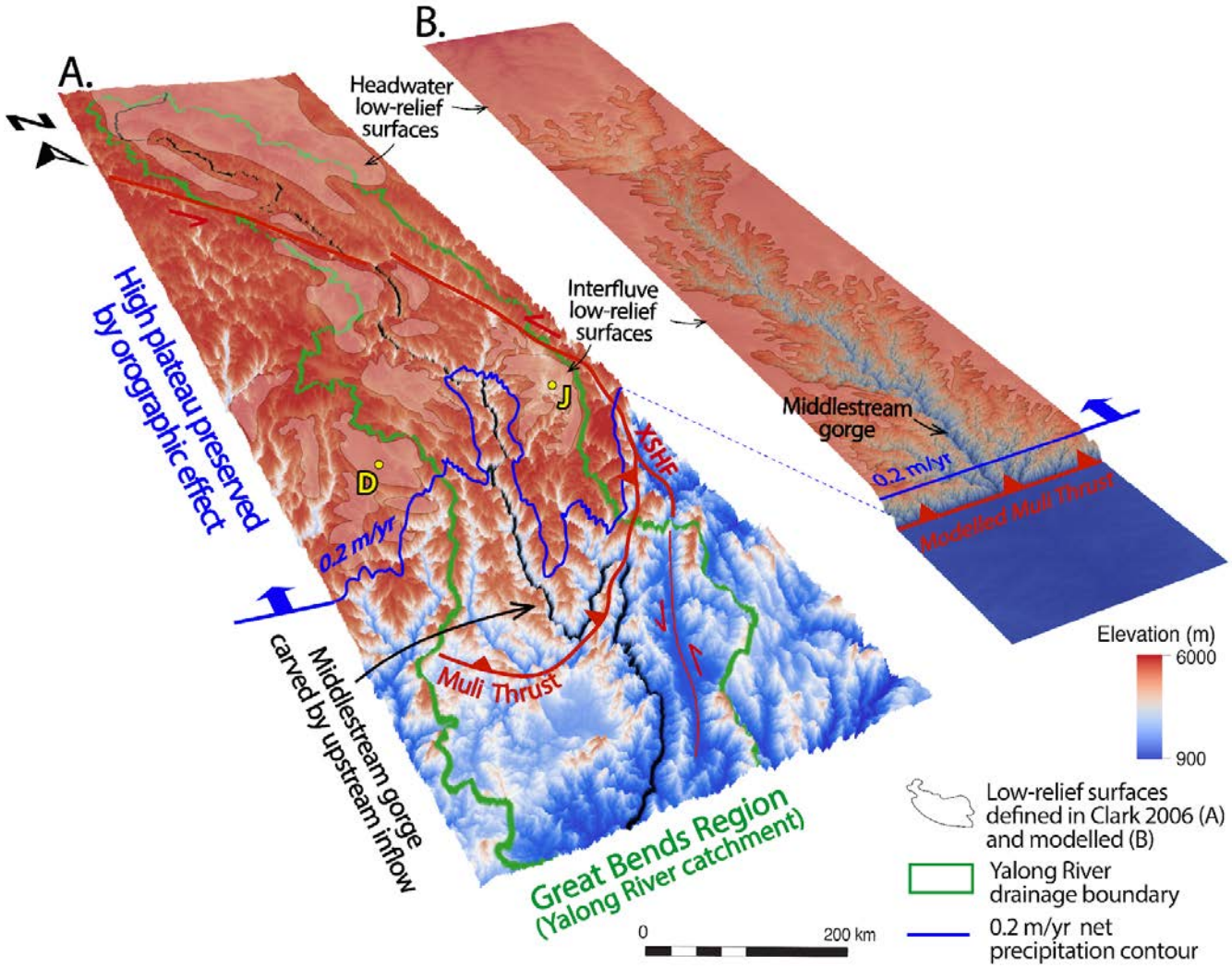

***Figure 8**: (A) Topography of Southeast Tibet showing the Yalong River catchment (in green) in the Great Bends Region. The net precipitation contour of 0.2 m/yr (in blue) roughly outlines the southeastern Tibetan Plateau edge. The low precipitation rate above this line (orographic effect) preserved from regressive erosion the emblematic low–relief and high–elevation Daocheng (D) and Jaggai (J) surfaces (in yellow) near the plateau edge. With a fast topographic uplift of the Yalong River catchment since ~15 Ma, in agreement with the fast exhumation rate of Muli thrust (red line), the main regional thrust, the orographic effect could be established since ~10 Ma, when the plateau elevation reaches ~2700 m. Xianshuihe Fault System (XFHS). (B) Final state topography of "Increasing upstream inflow scenario", in which a large amount of water collected in the upstream flat catchment allows abundant runoff in the river network and carves a deep gorge upstream of the Muli thrust, as observed for the Yalong River. Pale white shades in A (defined in Clark and al., 2006) and B (modelled) : low–relief surfaces.*

5.2 Implication of Oligocene versus Miocene rock uplift on the topography evolution of the Yalong catchment

Based on low temperature thermochronological data, the YTB has been invoked to explain the uplift history of the Yalong margin of Southeast Tibet, with strong activity since ~12.5 Ma (Clark et al., 2005; Pitard et al., 2021), or

~35 Ma (Zhang et al., 2016). We use these results to build two simplified tectonic models, the "Muli uplift" and "Jiulong uplift" scenarios, with uniform rock uplift starting at 15 or 30 Ma, respectively. We show that the "Muli uplift scenario" best reproduces the river profile morphology, while the longer rock uplift phase of the "Jiulong uplift scenario" with reduced rock uplift rate would result in an enhancement of erosion (Fig. 4). Therefore, we conclude that a predominant strong exhumation phase as estimated for the Muli thrust since the middle Miocene (Pitard et al., 2021) is mandatory to build the strong topographic step of the Yalong catchment (Fig. 1). In contrast, similar to the "Jiulong uplift scenario", the activity of the LMTB has been more intense during 30–25 Ma (exhumation rate 0.8 km/Myr) than since 10 Ma (exhumation rate 0.4 km/Myr) (Godard et al., 2009; Wang et al., 2012a). Such a longer tectonic phase would reinforce a regional fluvial erosion, with wider Dadu and Min rivers and a more developed dendritic drainage networks in the hinterland of the range when compared to the Yalong river catchment (Fig. 2). Indeed, the most emblematic high and low–relief surfaces located very close to the plateau edge, such as the Daocheng and Jaggai surfaces, are observed along the middlestream Yalong river gorge (Fig. 8), but none along the Dadu and Min rivers.

5.3 Modelling upstream water inflow collected from the low–relief high–elevation headwater, previously endorheic

The combination of a strong orographic effect, as observed today, and a fast recent regional rock uplift rate (Fig. 6 & S8) easily models the high–elevation, low–relief interfluve surfaces, such as the Daocheng and Jaggai surfaces, located close to the plateau edge and immediately above the 0.2 m/yr precipitation line (Fig. 8). In contrast, modelling the deeply–incised river valleys (~ 2500 m deep), as in the middlestream Yalong River, is complex and needs abundant runoff in the river network. The wide upstream flat catchment of the Yalong River allows a large amount of water to be collected in a single river, but without significantly eroding the upstream topography (Fig. 1). On this upstream flat catchment, evasive lacustrine sediments were reported to be deposited between ~23.5 Ma and ~13.5 Ma in numerous large interconnected paleo–lakes (Fig. 1B), before being captured from southeast by large externally drained rivers at ~11 Ma (Wu et al., 2008; Duvall et al., 2012). In the "Top–down incision scenario", the capture of the endorheic zone, reproduced as an upstream expansion of strong rainfall area, leads to a strong regressive erosion of the plateau, with concave–up river profiles (Fig. 5), no matter which K_f value or p is applied (Fig. S4). It forms upstream steep escarpments, similar to the one observed in passive continental margins along the coasts of southwest Africa and southeast of South America, which was interpreted as a long–existing "escarpment–retreat" (Braun, 2018). But such a steep upstream escarpment is not observed in the tectonically active Southeast Tibet. In the "Increasing upstream inflow scenario", we impose a strong water inflow in the uppermost part to add extra runoff and stream power in the channel. It is the only model to reproduce the narrowness of the Yalong River and the high k_{sn} values upstream of the YTB (Fig. 7). In addition, a long period of such strong upstream inflow (10-0 Ma) is needed to carve deep downstream gorge (Fig. S10D), which does not necessarily mimic a temporary lake draining (Wu et al., 2008; Rohrmann et al., 2023). It suggests a long–term and continuous process of collecting water on a wide flat headwater, which was previously endorheic. On such a wide and flat area, the diffusion or hillslope processes have to be dominant on the geomorphological landscape evolution. However, testing a more complex stream power law including a threshold parameter (τc) or different diffusion coefficient (Kd) values have not been conclusive (Fig. S10 & S11), considering that the diffusion processes have

typical lengths of an order of hundreds of meters, while we used a spatial resolution of 1000 m to model the continent–scale catchment of the Yalong River. A finer resolution would be promising to better model these processes and help to reproduce the flat slope in the upstream–most part of the Yalong River (Fig. 7), also observed for the Yangtze, Mekong and Salween rivers (Yang et al., 2016).

6. Conclusion

Southeast Tibet, externally drained by the large Salween, Mekong, Yangtze and Yalong rivers, is characterized by flat upstream areas on the inland plateau and low–relief interfluve surfaces at high elevation, bordering deep gorges across the plateau edge. We make numerical experiments to test several scenarios based on our geomorpho–tectonic analysis of the Yalong River drainage area. Our modelling results show that the previously suggested intensified monsoon since the Mid–Miocene Climate Optimum (~17–14 Ma) on the already–existing pre–Neogene high plateau would have destroyed the high plateau. Similarly, an expansion of drainage area by capturing the upstream endorheic zone of a high plateau since 15 Ma with intense precipitation would also have destroyed the high plateau. On the contrary, the orographic effect, which reduces the amount of precipitation on the plateau, preserved it from regressive erosion. Nevertheless, a long rock uplift phase (since ~30 Ma) would result in strong erosion of the topography, with large and wide rivers and no interfluve low–relief surfaces preserved at high elevation (as observed for the Dadu River), while a shorter rock uplift phase (since ~15 Ma), such as the Miocene activity revealed from the Muli thrust, is essential to preserve the elevated interfluve surfaces (as observed for the Yalong River). Furthermore, considering only the orographic effect on reducing precipitation on the plateau would result in a weak net precipitation, which could not generate enough runoff to sufficiently incise in river channels. Conclusively, we propose that, in the Great Bends Region, a combination of strong Miocene rock uplift, weak net precipitation on the high plateau above 2700 m as observed today, and an increasing channel inflow, due to large amount of water collected from capturing a formerly large endorheic zone of inland plateau, well reproduces the headwater and interfluve low–relief surfaces and deeply incised rivers in the Yalong River catchment.

Acknowledgements

This work has been supported by the China Scholarship Council Funds and Agence Nationale de Recherche (ANR-20-CE49-0008_Tibetan-Orchestra). Jean Braun is warmly thanked for providing the FastScape code and constructive comments on the modelling. Thanks to Peter van der Beek for very helpful discussion and correction of the manuscript. We thank the anonymous reviewers for constructive comments that improved the manuscript.

Author contribution

OX and AR have worked together through this manuscript.

Declaration of competing interest

The authors declare that there are no known competing financial interests or personal relationships that could have influenced this paper.

Table 1

Parameters for model setup

Notation	Definition	Value/Range	Unit
h	topography elevation		m
$\triangle$	incremental time	200000	yr
n_{steps}	Total run steps	250	–
x	width	200	km
y	length	1250	km
$\triangle x, \triangle y$	pixel size	1	km
U	rock uplift rate	0.13, 0.24	m/yr
p	net precipitation rate	0–1	m/yr
A	drainage area		m^2
S	slope in flow direction		–
m	stream power law exponent	0.4	–
n	stream power law exponent	1	–
K_f	erosion coefficient	$2–6\times10^{-6}$	$m^{0.2}/yr$
K_d	hillslope diffusion coefficient	0–0.1	m^2/yr
base_level	fixed height boundary	900	m

References

Ahnert, F., 1967. The Role of the Equilibrium Concept in the Interpretation of Landforms of Fluvial Erosion and Deposition.

Armitage, T.W.K., Kwok, R., Thompson, A.F., Cunningham, G., 2018. Dynamic Topography and Sea Level Anomalies of the Southern Ocean: Variability and Teleconnections. Journal of Geophysical Research: Oceans 123, 613-630. https://doi.org/10.1002/2017JC013534

Braun, J., Willett, S.D., 2013. A very efficient O(n), implicit and parallel method to solve the stream power equation governing fluvial incision and landscape evolution. Geomorphology 180-181, 170-179. http://dx.doi.org/10.1016/j.geomorph.2012.10.008

Braun, J., 2018. A review of numerical modeling studies of passive margin escarpments leading to a new analytical expression for the rate of escarpment migration velocity. Gondwana Research 53, 209-224. https://doi.org/10.1016/j.gr.2017.04.012

Cao, K., Wang, G., Leloup, P.H., Mahéo, G., Xu, Y., van der Beek, P.A., Replumaz, A., Zhang, K., 2019. Oligocene-Early Miocene Topographic Relief Generation of Southeastern Tibet Triggered by Thrusting. Tectonics 38, 374-391. https://doi.org/10.1029/2017TC004832

Cao, K., Leloup, P.H., Wang, G., Liu, W., Mahéo, G., Shen, T., Xu, Y., Sorrel, P., Zhang, K., 2020. Thrusting, exhumation, and basin fill on the western margin of the South China block during the India-Asia collision. GSA Bulletin 133, 74-90. https://doi.org/10.1130/B35349.1

Clark, M.K., Royden, L.H., 2000. Topographic ooze: Building the eastern margin of Tibet by lower crustal flow. Geology 28, 703-706. https://doi.org/10.1130/0091-7613(2000)28

Clark, M.K., House, M., Royden, L., Whipple, K., Burchfiel, B., Zhang, X., Tang, W., 2005. Late Cenozoic uplift of southeastern Tibet. Geology 33, 525-528. https://doi.org/10.1130/G21265.1

Clark, M.K., Schoenbohm, L.M., Royden, L.H., Whipple, K.X., Burchfiel, B.C., Zhang, X., Tang, W., Wang, E., Chen, L., 2004. Surface uplift, tectonics, and erosion of eastern Tibet from large-scale drainage patterns. Tectonics 23. https://doi.org/10.1029/2002TC001402

Clift, P.D., 2006. Controls on the erosion of Cenozoic Asia and the flux of clastic sediment to the ocean. Earth and Planetary Science Letters 241, 571-580. https://doi.org/10.1016/j.epsl.2005.11.028

Clift, P.D., Giosan, L., 2014. Sediment fluxes and buffering in the post-glacial Indus Basin. Basin Research 26, 369-386. https://doi.org/10.1111/bre.12038

Densmore, A.L., Allen, P. a., Simpson, G., 2007. Development and response of a coupled catchment fan system under changing tectonic and climatic forcing. Journal of Geophysical Research: Earth Surface 112, 1-16. https://doi.org/10.1029/2006JF000474

Duvall, A.R., Clark, M.K., Avdeev, B., Farley, K.A., Chen, Z., 2012. Widespread late Cenozoic increase in erosion rates across the interior of eastern Tibet constrained by detrital low-temperature thermochronometry. Tectonics 31. https://doi.org/10.1029/2011TC002969

Fang, X., Yan, M., Zhang, W., Nie, J., Han, W., Wu, F., Song, C., Zhang, T., Zan, J., Yang, Y., 2021. Paleogeography control of Indian monsoon intensification and expansion at 41 Ma. Science Bulletin 66, 2320-2328. https://doi.org/10.1016/j.scib.2021.07.023

Fox, M., Carter, A., Dai, J.-G., 2020. How Continuous Are the "Relict" Landscapes of Southeastern Tibet? Frontiers in Earth Science 8. https://doi.org/10.3389/feart.2020.587597

Godard, V., Pik, R., Lavé, J., Cattin, R., Tibari, B., de Sigoyer, J., Pubellier, M., Zhu, J., 2009. Late Cenozoic evolution of the central Longmen Shan, eastern Tibet: Insight from (U-Th)/He thermochronometry. Tectonics 28. https://doi.org/10.1029/2008TC002407

Gourbet, L., Leloup, P.H., Paquette, J.-L., Sorrel, P., Maheo, G., Wang, G., Yadong, X., Cao, K., Antoine, P.-O., Eymard, I., Liu, W., Lu, H., Replumaz, A., Chevalier, M.-L., Kexin, Z., Jing, W., Shen, T., 2017. Reappraisal of the Jianchuan Cenozoic basin stratigraphy and its implications on the SE Tibetan plateau evolution. Tectonophysics 700-701, 162-179. https://doi.org/10.1016/j.tecto.2017.02.007

Guo, Z.T., Ruddiman, W.F., Hao, Q.Z., Wu, H.B., Qiao, Y.S., Zhu, R.X., Peng, S.Z., Wei, J.J., Yuan, B.Y., Liu, T.S., 2002. Onset of Asian desertification by 22 Myr ago inferred from loess deposits in China. Nature 416, 159-163. https://doi.org/10.1038/416159a

Guo, Z.T., Sun, B., Zhang, Z.S., Peng, S.Z., Xiao, G.Q., Ge, J.Y., Hao, Q.Z., Qiao, Y.S., Liang, M.Y., Liu, J.F., 2008. A major reorganization of Asian climate by the early Miocene. Climate of the Past 4, 153-174. https://doi.org/10.5194/cp-4-153-2008

Hallet, B., Molnar, P., 2001. Distorted drainage basins as markers of crustal strain east of the Himalaya. Journal of Geophysical Research: Solid Earth 106, 13697-13709. https://doi.org/10.1029/2000JB900335

Hoke, G.D., Liu-Zeng, J., Hren, M.T., Wissink, G.K., Garzione, C.N., 2014. Stable isotopes reveal high southeast Tibetan Plateau margin since the Paleogene. Earth and Planetary Science Letters 394, 270-278. https://doi.org/10.1016/j.epsl.2014.03.007

Howard, A.D., Kerby, G., 1983. Channel changes in badlands. GSA Bulletin 94, 739-752. https://doi.org/10.1130/0016-7606(1983)94<739:CCIB>2.0.CO;2

Kirby, E., Whipple, K.X., 2012. Expression of active tectonics in erosional landscapes. Journal of Structural Geology 44, 54-75. https://doi.org/10.1016/j.jsg.2012.07.009

Lague, D., Hovius, N., Davy, P., 2005. Discharge, discharge variability, and the bedrock channel profile. Journal of Geophysical Research: Earth Surface 110. https://doi.org/10.1029/2004JF000259

Li, S., Currie, B.S., Rowley, D.B., Ingalls, M., 2015a. Cenozoic paleoaltimetry of the SE margin of the Tibetan Plateau: Constraints on the tectonic evolution of the region. Earth and Planetary Science Letters 432, 415-424. https://doi.org/10.1016/j.epsl.2015.09.044

Li, S., Deng, C., Dong, W., Sun, L., Liu, S., Qin, H., Yin, J., Ji, X., Zhu, R., 2015b. Magnetostratigraphy of the Xiaolongtan Formation bearing Lufengpithecus keiyuanensis in Yunnan, southwestern China: Constraint on

the initiation time of the southern segment of the Xianshuihe–Xiaojiang fault. Tectonophysics 655, 213-226. https://doi.org/10.1016/j.tecto.2015.06.002

Liu-Zeng, J., Tapponnier, P., Gaudemer, Y., Ding, L., 2008. Quantifying landscape differences across the Tibetan plateau: Implications for topographic relief evolution. Journal of Geophysical Research: Earth Surface 113. https://doi.org/10.1029/2007JF000897

Martin, Y., 2000. Modelling hillslope evolution: linear and nonlinear transport relations. Geomorphology 34, 1-21. https://doi.org/10.1016/S0169-555X(99)00127-0

Nie, J., Ruetenik, G., Gallagher, K., Hoke, G., Garzione, C.N., Wang, W., Stockli, D., Hu, X., Wang, Z., Wang, Y., Stevens, T., Danišík, M., Liu, S., 2018. Rapid incision of the Mekong River in the middle Miocene linked to monsoonal precipitation. Nature Geoscience 11, 944-948. https://doi.org/10.1038/s41561-018-0244-z

Ou, X., Replumaz, A., van der Beek, P., 2021. Contrasting exhumation histories and relief development within the Three Rivers Region (south-east Tibet). Solid Earth 12, 563-580. https://doi.org/10.5194/se-12-563-2021

Perron, J.T., Royden, L., 2013. An integral approach to bedrock river profile analysis. Earth Surface Processes and Landforms 38, 570-576. https://doi.org/10.1002/esp.3302

Pitard, P., Replumaz, A., Chevalier, M.-L., Leloup, P.-H., Bai, M., Doin, M.-P., Thieulot, C., Ou, X., Balvay, M., Li, H., 2021. Exhumation History Along the Muli Thrust—Implication for Crustal Thickening Mechanism in Eastern Tibet. Geophysical Research Letters 48, e2021GL093677. https://doi.org/10.1029/2021GL093677

Replumaz, A., San José, M., Margirier, A., van der Beek, P., Gautheron, C., Leloup, P.H., Ou, X., Kai, C., Wang, G.-C., Zhang, Y.-Z., Valla, P.G., Balvay, M., 2020. Tectonic Control on Rapid Late Miocene—Quaternary Incision of the Mekong River Knickzone, Southeast Tibetan Plateau. Tectonics 39, e2019TC005782. https://doi.org/10.1029/2019TC005782

Rohrmann, A., Schwanghart, W., Kirby, E., 2018. Yangtze upstream-river network expansion reveals potential top-down incision, pp. EP53A-03.

Rohrmann, A., Schwanghart, W., Kirby, E., 2023. Accelerated Miocene incision along the Yangtze River driven by headward drainage basin expansion. Sci. Adv. 9, eadh1636. https://doi.org/10.1126/sciadv.adh1636

Royden, L.H., Burchfiel, B.C., King, R.W., Wang, E., Chen, Z., Shen, F., Liu, Y., 1997. Surface Deformation and Lower Crustal Flow in Eastern Tibet. Science 276, 788-790. https://doi.org/10.1126/science.276.5313.788

Schwanghart, W., Scherler, D., 2014. Short Communication: TopoToolbox 2 – MATLAB-based software for topographic analysis and modeling in Earth surface sciences. Earth Surf. Dynam. 2, 1-7. https://doi.org/10.5194/esurf-2-1-2014

Sorrel, P., Eymard, I., Leloup, P.-H., Maheo, G., Olivier, N., Sterb, M., Gourbet, L., Wang, G., Jing, W., Lu, H., Li, H., Yadong, X., Zhang, K., Cao, K., Chevalier, M.-L., Replumaz, A., 2017. Wet tropical climate in SE Tibet during the Late Eocene. Scientific Reports 7, 7809. https://doi.org/10.1038/s41598-017-07766-9

Stock, J.D., Montgomery, D.R., 1999. Geologic constraints on bedrock river incision using the stream power law. Journal of Geophysical Research: Solid Earth 104, 4983-4993. https://doi.org/10.1029/98JB02139

Su, T., Farnsworth, A., Spicer, R.A., Huang, J., Wu, F.-X., Liu, J., Li, S.-F., Xing, Y.-W., Huang, Y.-J., Deng, W.-Y.-D., Tang, H., Xu, C.-L., Zhao, F., Srivastava, G., Valdes, P.J., Deng, T., Zhou, Z.-K., 2019. No high Tibetan Plateau until the Neogene. Science Advances 5, eaav2189. https://doi.org/10.1126/sciadv.aav2189

Tang, M., Liu-Zeng, J., Hoke, G.D., Xu, Q., Wang, W., Li, Z., Zhang, J., Wang, W., 2017. Paleoelevation reconstruction of the Paleocene-Eocene Gonjo basin, SE-central Tibet. Tectonophysics 712-713, 170-181. https://doi.org/10.1016/j.tecto.2017.05.018

Wang, E., Kirby, E., Furlong, K.P., van Soest, M., Xu, G., Shi, X., Kamp, P.J.J., Hodges, K.V., 2012a. Two-phase growth of high topography in eastern Tibet during the Cenozoic. Nature Geoscience 5, 640-645. https://doi.org/10.1038/ngeo1538

Wang, S., Jiang, G., Xu, T., Tian, Y., Zheng, D., Fang, X., 2012b. The Jinhe–Qinghe fault—An inactive branch of the Xianshuihe–Xiaojiang fault zone, Eastern Tibet. Tectonophysics 544-545, 93-102. https://doi.org/10.1016/j.tecto.2012.04.004

Whipple, K.X., Tucker, G.E., 1999. Dynamics of the stream-power river incision model: Implications for height limits of mountain ranges, landscape response timescales, and research needs. Journal of Geophysical Research: Solid Earth 104, 17661-17674. https://doi.org/10.1029/1999JB900120

Wobus, C., Whipple, K.X., Kirby, E., Snyder, N., Johnson, J., Spyropolou, K., Crosby, B., Sheehan, D., Willett, S.D., Hovius, N., Brandon, M.T., Fisher, D.M., 2006. Tectonics from topography: Procedures, promise, and pitfalls, Tectonics, Climate, and Landscape Evolution. Geological Society of America, p. 0. https://doi.org/10.1130/2006.2398(04)

Wu, Z., Barosh, P.J., Zhonghai, W., Daogong, H., Xun, Z., Peisheng, Y., 2008. Vast early Miocene lakes of the central Tibetan Plateau. GSA Bulletin 120, 1326-1337. https://doi.org/10.1130/B26043.1

Xiong, Z., Ding, L., Spicer, R.A., Farnsworth, A., Wang, X., Valdes, P.J., Su, T., Zhang, Q., Zhang, L., Cai, F., Wang, H., Li, Z., Song, P., Guo, X., Yue, Y., 2020. The early Eocene rise of the Gonjo Basin, SE Tibet: From low desert to high forest. Earth and Planetary Science Letters 543, 116312. https://doi.org/10.1016/j.epsl.2020.116312

Yang, R., Fellin, M.G., Herman, F., Willett, S.D., Wang, W., Maden, C., 2016. Spatial and temporal pattern of erosion in the Three Rivers Region, southeastern Tibet. Earth and Planetary Science Letters 433, 10-20. https://doi.org/10.1016/j.epsl.2015.10.032

Yang, R., Willett, S.D., Goren, L., 2015. In situ low-relief landscape formation as a result of river network disruption. Nature 520, 526-529. https://doi.org/10.1038/nature14354

Yuan, X., Jiao, R., Dupont-Nivet, G., Shen, X., 2022. Southeastern Tibetan Plateau growth revealed by inverse analysis of landscape evolution model. Geophysical Research Letters 49, e2021GL097623. https://doi.org/10.1029/2021GL097623

Yuan, X.P., Huppert, K.L., Braun, J., Shen, X., Liu-Zeng, J., Guerit, L., Wolf, S.G., Zhang, J.F., Jolivet, M., 2021. Propagating uplift controls on high-elevation, low-relief landscape formation in the southeast Tibetan Plateau. Geology 50, 60-65. https://doi.org/10.1130/G49022.1

Yuan, X., Jiao, R., J. Liu-Zeng, Dupont-Nivet, G., Wolf, S.G. Shen, X., 2023. Downstream propagation of fluvial erosion in Eastern Tibet. Earth and Planetary Science Letters, Volume 605, 118017, https://doi.org/10.1016/j.epsl.2023.118017

Zhang, Y.-Z., Replumaz, A., Wang, G.-C., Leloup, P.H., Gautheron, C., Bernet, M., van der Beek, P., Paquette, J.L., Wang, A., Zhang, K.-X., Chevalier, M.-L., Li, H.-B., 2015. Timing and rate of exhumation along the Litang fault system, implication for fault reorganization in Southeast Tibet. Tectonics 34, 1219-1243. https://doi.org/10.1002/2014TC003671

Zhang, H., Oskin, M.E., Liu-Zeng, J., Zhang, P., Reiners, P.W., Xiao, P., 2016. Pulsed exhumation of interior eastern Tibet: Implications for relief generation mechanisms and the origin of high-elevation planation surfaces. Earth and Planetary Science Letters 449, 176-185. https://doi.org/10.1016/j.epsl.2016.05.048

Zhang, G., Tian, Y., Li, R., Shen, X., Zhang, Z., Sun, X., Chen, D., 2022. Progressive tectonic evolution from crustal shortening to mid-lower crustal expansion in the southeast Tibetan Plateau: A synthesis of structural and thermochronological insights. Earth-Science Reviews 226, 103951. https://doi.org/10.1016/j.earscirev.2022.103951

Zheng, H., Yang, Q., Cao, S., Clift, P.D., He, M., Kano, A., Sakuma, A., Xu, H., Tada, R., Jourdan, F., 2022. From desert to monsoon: irreversible climatic transition at ~ 36 Ma in southeastern Tibetan Plateau. Progress in Earth and Planetary Science 9, 12. https://doi.org/10.1186/s40645-022-00470-x

Zhu, C., Wang, G., Leloup, P.H., Cao, K., Mahéo, G., Chen, Y., Zhang, P., Shen, T., Wu, G., Sotiriou, P., Wu, B., 2021. Role of the Early Miocene Jinhe-Qinghe Thrust Belt in the building of the Southeastern Tibetan Plateau topography. Tectonophysics 811, 228871. https://doi.org/10.1016/j.tecto.2021.228871